



HAL
open science

Gravitational lensing effects of supermassive black holes in cluster environments

Guillaume Mahler, Priyamvada Natarajan, Mathilde Jauzac, Johan Richard

► **To cite this version:**

Guillaume Mahler, Priyamvada Natarajan, Mathilde Jauzac, Johan Richard. Gravitational lensing effects of supermassive black holes in cluster environments. *Monthly Notices of the Royal Astronomical Society*, 2023, 518 (1), pp.54-65. 10.1093/mnras/stac3098 . hal-03566485

HAL Id: hal-03566485

<https://hal.science/hal-03566485v1>

Submitted on 15 Feb 2024

HAL is a multi-disciplinary open access archive for the deposit and dissemination of scientific research documents, whether they are published or not. The documents may come from teaching and research institutions in France or abroad, or from public or private research centers.

L'archive ouverte pluridisciplinaire **HAL**, est destinée au dépôt et à la diffusion de documents scientifiques de niveau recherche, publiés ou non, émanant des établissements d'enseignement et de recherche français ou étrangers, des laboratoires publics ou privés.



Distributed under a Creative Commons Attribution 4.0 International License

Gravitational lensing effects of supermassive black holes in cluster environments

Guillaume Mahler ^{1,2★}, Priyamvada Natarajan ^{3,4,5}, Mathilde Jauzac ^{1,2,6,7} and Johan Richard ⁸

¹*Institute for Computational Cosmology, Durham University, South Road, Durham DH1 3LE, UK*

²*Centre for Extragalactic Astronomy, Durham University, South Road, Durham DH1 3LE, UK*

³*Department of Astronomy, Yale University, 52 Hillhouse Avenue, New Haven, CT 06511, USA*

⁴*Department of Physics, Yale University, P.O. Box 208121, New Haven, CT 06520, USA*

⁵*Black Hole Initiative, Harvard University, 20 Garden Street, Cambridge, MA 02138, USA*

⁶*Astrophysics Research Centre, University of KwaZulu-Natal, Westville Campus, Durban 4041, South Africa*

⁷*School of Mathematics, Statistics & Computer Science, University of KwaZulu-Natal, Westville Campus, Durban 4041, South Africa*

⁸*Univ Lyon, Univ Lyon1, Ens de Lyon, CNRS, Centre de Recherche Astrophysique de Lyon UMR5574, F-69230 Saint-Genis-Laval, France*

Accepted 2022 October 20. Received 2022 October 17; in original form 2022 January 26

ABSTRACT

This study explores the gravitational lensing effects of supermassive black holes (SMBHs) in galaxy clusters. While the presence of central SMBHs in galaxies is firmly established, recent work from high-resolution simulations predict the existence of an additional population of wandering SMBHs. Though the masses of these SMBHs are a minor perturbation on the larger scale and individual galaxy scale dark matter components in the cluster, they can impact statistical lensing properties and individual lensed image configurations. Probing for these potentially observable signatures, we find that SMBHs imprint detectable signatures in rare, higher order strong lensing image configurations although they do not manifest any statistically significant detectable evidence in either the magnification distribution or the integrated shear profile. Investigating specific lensed image geometries, we report that a massive, near point-like, potential of an SMBH causes the following detectable effects: (i) image splitting leading to the generation of extra images; (ii) positional and magnification asymmetries in multiply imaged systems; and (iii) the apparent disappearance of a lensed counter image. Of these, image splitting inside the cluster tangential critical curve, is the most prevalent notable observational signature. We demonstrate these possibilities in two cases of observed giant arcs in SGAS J003341.5+024217 and RX J1347.5–1145, wherein specific image configurations seen can be reproduced with SMBHs. Future observations with high-resolution instrumentation (e.g. MAVIS-Very Large Telescope, MICADO-Extremely Large Telescope, and the upgraded ngVLA, along with data from the *Euclid* and *Nancy Grace Roman* Space Telescopes and the Rubin LSST Observatory are likely to allow us to probe these unique yet rare SMBHs lensing signatures.

Key words: black hole physics – gravitational lensing: strong – galaxies: clusters: general – galaxies: elliptical and lenticular, cD – cosmology: observations – dark matter.

1 INTRODUCTION

Gravitational lensing has emerged as a powerful method to probe the detailed mass distribution on multiple cosmic scales in the Universe, from individual galaxies, groups of galaxies to clusters of galaxies, which all serve as effective lenses for the distant background galaxies and quasars (see review by Kneib & Natarajan 2011 for details). We now know that most, if not all, galaxies in the Universe likely harbour a central supermassive black hole (SMBH). SMBHs are ubiquitous at the centres of galaxies, and the most massive ones are expected in the brightest cluster galaxies (BCGs) that anchor the centre of the gravitational potential well in galaxy clusters. Observations suggest that properties of central SMBHs are correlated to properties of their host galaxy (Magorrian et al. 1998; Ferrarese & Merritt 2000; Gebhardt et al. 2000; Tremaine et al. 2002). Even though the mass of

the central SMBH is negligible compared to the mass of the stellar component of its host galaxy, in just the bulge $M_{\text{bh}} \sim 10^{-3} M_{\text{bulge}}$, coupling scales the SMBH nevertheless appears to play an important role in modulating star formation in the galactic nucleus.

Gravitational lensing, predicted by General Relativity results in the deflection of light paths by strong gravitational potentials encountered en-route. Light from distant background galaxies is deflected by the foreground potential of a galaxy cluster and its member galaxies producing a multiplicity of detectable effects. Gravitational lensing observations provide strong constraints on the inner density profiles of galaxies and clusters due to the production of multiple images and highly magnified distorted arcs. In this paper, we explore the gravitational lensing effects produced by SMBHs in cluster environments.

Lensing theory predicts that for simple isolated galaxy lenses every strong lensing system should produce a faint, demagnified image at the very inner centre of the lens. However, these central images have only been hinted (Winn, Rusin & Kochanek 2004) in lensed radio

* E-mail: guillaume.mahler@durham.ac.uk

galaxies and multiple studies have focused on them as there is scarce contamination by the lens itself (e.g. Winn et al. 2004; Rusin, Keeton & Winn 2005; Tamura et al. 2015; Wong, Suyu & Matsushita 2015; Quinn et al. 2016; Wong et al. 2017).

Realistic models of galaxies with a dominant central stellar component predict a wide range of properties for these core images spanning a range of magnification factors. Despite systematic searches for these central de-magnified images, they have not been found. While tweaking properties of the stellar component can account for the absence of these images, Mao, Witt & Koopmans (2001) showed that the presence of a central SMBH introduces new qualitative features in the resulting critical and caustic curves that could easily destroy the presence of these central images.

Traditionally, the detection of active SMBHs has been through X-ray studies of the accretion process that has permitted mass measurements. For nearby, dormant SMBHs, their masses have been successfully constrained mapping the gravitational potential using stars and gas when available as tracers. However, the kind of data needed for dynamical modelling to determine SMBH masses is unavailable for sources beyond 50–100 Mpc. Since lensing is achromatic, mapping the shadow of gas accretion including lensing effects close to the horizon, recently permitted the Event Horizon Telescope (EHT) Collaboration to garner a mass measurement for the SMBH at the centre of M87. The central SMBH in M87 is reported to have a mass of $6.5 \times 10^9 M_{\odot}$ Event Horizon Telescope Collaboration (2019). While such measurements are infeasible for $z > 0.1$ SMBHs, lensing effects resolvable with the next generation of interferometric radio arrays like the ngVLA might provide an entirely new method to measure SMBH masses. It is this, in part, that motivates our current study. In particular, if any unique detectable SMBH lensing signatures exist, they would offer a novel way to find dormant SMBHs at intermediate redshifts, $0.2 < z < 1.0$, and serve as invaluable addition to our understanding of the growth and evolution black hole populations over cosmic time.

Previous theoretical work has focused on including the presence of a central SMBH in the galactic nucleus of an individual galaxy lens. The gravitational potential of an SMBH was added to various assumed galaxy mass profiles, ranging from a cored isothermal sphere (Mao et al. 2001) and a Plummer model (Werner & Evans 2006) to explore their combined lensing effects. Recently, Karamazov, Timko & Heyrovsky (2021) include the central SMBH as a point mass embedded in an NFW profile to model the BCG in a fiducial galaxy cluster.

Given the clear cut prediction of the absence of the central image in the case of isolated galaxies, various groups including Keeton (2003), Chen et al. (2018), and Inada et al. (2008) have looked at optical and radio data of distant galaxies ($z \sim 0.2$ –1) to search for the central image. Multiple studies have been focused on lensed radio galaxies as there is no contamination by the lens itself (e.g. Winn et al. 2004; Rusin et al. 2005; Tamura et al. 2015; Wong et al. 2015, 2017; Quinn et al. 2016). While these de-magnified images remain undetected, this absence of detection in itself is not a clear cut signal telegraphing the presence of a central SMBH. In fact, Smith, Lucey & Edge (2017) showed that a change in the stellar IMF can also alter the central density of the stellar component in the inner regions of galaxies sufficiently to remove central images. Therefore, the absence of a central image cannot be assumed to provide smoking gun evidence for an SMBH. Central images could appear more clearly in lensing potential embedded in more complex environment as it could shift demagnification region outside the inner core of the galaxy (e.g. Dahle et al. 2013; Sharon et al. 2017; Ostrovski et al. 2018; Muller et al. 2020; Martinez et al. 2022).

Additionally, the presence of dark substructures (whose lensing effects would be degenerate with that of SMBHs) have also been inferred from galaxy–galaxy lensing studies, as reported in Minor et al. (2021a,b) where they argue for evidence of the existence of massive compact sub-haloes perturbing the observed lensing signal. In the latter case, an associated, luminous counterpart is seen but that could also be related to additional sources lensed behind (Collett & Smith 2020; Smith & Collett 2021).

In the work presented in this paper, we extend and expand previous studies to examine in detail the lensing signatures SMBHs in a range of cluster environments: the case of a central SMBH in a cluster BCG; a central SMBH in a cluster member galaxy, and the more general case of a wandering SMBH in the cluster environment. We are motivated to study the effect of this additional wandering SMBH population due to recent work by Ricarte et al. (2021a,b). Analysing a high-resolution simulated cluster, Romulus-C, (Ricarte et al. 2021a) reported the existence of a large population of wandering SMBHs in cluster environments originating from the tidal stripping and disruption of in-falling dwarf galaxies. In addition, microlensing in clusters is very sensitive to the mass but remains a very rare event, though recently Dai & Miralda-Escudé (2020) argue that significant monitoring of subtle changes in the magnification would be able to yield accurate mass measurements leading to the potential implication of IMBHs or SMBHs. Previous reports using microlensing events by stars in clusters (e.g. Icarus and Iapix in MACSJ1149 – Diego et al. 2018; Kelly et al. 2018) have been searched for.

The plan of our paper is as follows: in Section 2, we present the methods used to model and study the lensing effects of SMBHs in clusters; the lensing effects of the central BCG SMBHs, the central SMBHs in cluster galaxies, and wandering SMBHs are explored in Sections 3, 4, and 5, respectively. The impact of SMBHs on specific lensing image configurations is studied in detail and presented in Section 6, and the observational case studies in current data wherein SMBHs may be implicated are discussed in Section 7. We conclude in Section 8 with the prospects for future detection and delineation of SMBH lensing with the upcoming data deluge from new facilities.

2 MODELLING THE LENSING EFFECTS OF SMBHS

Here, we look more exhaustively at the range of lensing phenomena that could be revealed with the explicit inclusion of a central SMBH in a cluster galaxy or wandering SMBHs in clusters. We model the gravitational potential of the entire system holistically following (Natarajan & Kneib 1997) as a superposition of the following components: larger scale smooth components (that model the distribution of the smoothly distributed dark matter); a sum over galaxy-scale perturbers (that model the contribution of the dark matter subhaloes associated with individual cluster galaxies) and now explicitly include the associated SMBH population (those hosted at the centres of cluster galaxies or as wanderers) as

$$\phi = \phi_{\text{smooth}} + \sum_i \phi_{\text{clusgal}} + \sum_j \phi_{\text{BH}}. \quad (1)$$

As detailed below, we use mass profiles whose lensing properties are well understood to model mass components above.

2.1 Modelling the composite profile

To allow flexibility in our computation, we derive lensing properties adopting a dual pseudo-isothermal elliptical profile (dPIE; Kassiola & Kovner 1993; Natarajan & Kneib 1997; Elíasdóttir et al. 2007)

often used in lensing analysis. We use this profile to model cluster haloes, galaxy haloes, and SMBHs. This profile has the advantage that the first and second partial derivatives of the lensing potential can both be written out analytically. In addition, this profile offers a critical free parameter, the core radius, that can be tuned to flatten the central density distribution flexibly, that is of great utility while modelling the effect of SMBHs.

The 3D density distribution of the dPIE is given by

$$\rho(r) = \frac{\rho_0}{\left(1 + \left(\frac{r}{r_{\text{core}}}\right)^2\right)\left(1 + \left(\frac{r}{r_{\text{cut}}}\right)^2\right)}; r_{\text{cut}} > r_{\text{core}}. \quad (2)$$

Following the details presented in appendix A of Elíasdóttir et al. (2007), we adopt a fiducial central velocity dispersion σ_{dPIE} to relate to the central density as follows:

$$\sigma_{\text{dPIE}}^2 = \frac{4}{3} G \pi \rho_0 \frac{r_{\text{core}}^2 r_{\text{cut}}^3}{(r_{\text{cut}} - r_{\text{core}})(r_{\text{cut}} + r_{\text{core}})^2}. \quad (3)$$

The convergence, κ , and the shear, γ , of a single dPIE are given by

$$\kappa(R) \equiv \frac{\Sigma(R)}{\Sigma_{\text{crit}}} = \frac{\Sigma_0}{\Sigma_{\text{crit}}} \frac{r_{\text{core}} r_{\text{cut}}}{r_{\text{cut}} - r_{\text{core}}} \times \left(\frac{1}{\sqrt{r_{\text{core}}^2 + R^2}} - \frac{1}{\sqrt{r_{\text{cut}}^2 + R^2}} \right), \quad (4)$$

and

$$\gamma(R) = \frac{\Sigma_0}{\Sigma_{\text{crit}}} \frac{r_{\text{core}} r_{\text{cut}}}{r_{\text{cut}} - r_{\text{core}}} \left[2 \left(\frac{1}{r_{\text{core}} + \sqrt{r_{\text{core}}^2 + R^2}} - \frac{1}{r_{\text{cut}} + \sqrt{r_{\text{cut}}^2 + R^2}} \right) + \left(\frac{1}{\sqrt{r_{\text{core}}^2 + R^2}} - \frac{1}{\sqrt{r_{\text{cut}}^2 + R^2}} \right) \right] \quad ((6))$$

with

$$\Sigma_0 = \pi \rho_0 \frac{r_{\text{core}} r_{\text{cut}}}{r_{\text{cut}} + r_{\text{core}}} \quad (6)$$

$$\Sigma_{\text{crit}} \equiv \frac{c^2}{4\pi G} \frac{D_S}{D_L D_{LS}}, \quad (7)$$

where D_L , D_S , and D_{LS} are the angular diameter distances from the observer to the lens, the observer to the source, and between the lens and source, respectively.

2.2 Explicit inclusion of the SMBH component

We define the black hole mass hosted in a cluster galaxy by adopting the fiducial velocity dispersion of a dPIE profile as the central velocity of the bulge of the host galaxy. We can therefore, use the well-known empirically derived local black hole mass–bulge mass relation (Gültekin et al. 2009):

$$\text{Log} \left(\frac{M_{\text{bh}}}{M_{\odot}} \right) = \alpha + \beta * \text{Log} \left(\frac{\sigma_{\text{bulge}}}{200 \text{ km s}^{-1}} \right), \quad (8)$$

where $\alpha = 8.12$, $\beta = 4.24$, and σ_{bulge} is the bulge velocity dispersion defined here as the dPIE velocity dispersion shown in equation (3).

We then correlate the mass of a central SMBH to the dPIE profile to compute the lensing effect of the SMBH. Using a circularly symmetric profile, we adopt a cut radius of $r_{\text{cut}} = 1.0 \text{ pc}$, and a core radius of $r_{\text{core}} = 0.001 \text{ pc}$. These values are taken to account for an small accretion discs around the SMBH but its size is negligible for the current observations considered later in this analysis. The top panel of Fig. 1 shows the integrated mass profile of such a potential normalized by its total mass. This corresponds to roughly 99.8 per cent of the mass within the 330 pc corresponding to ~ 0.1

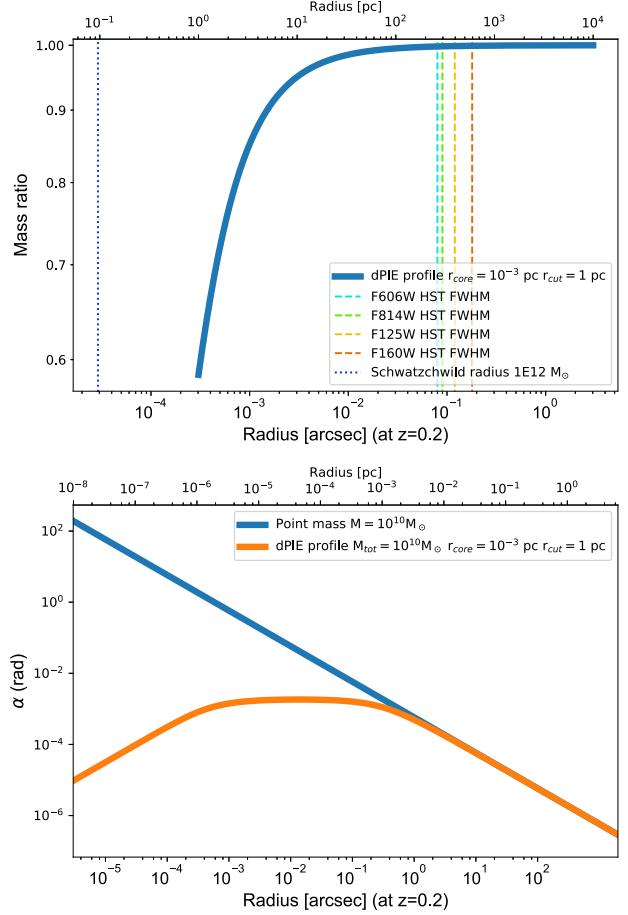


Figure 1. Top: Mass profile of a dPIE potential mimicking an SMBH normalized by the total mass with a cut radius of $r_{\text{cut}} = 1 \text{ pc}$ and a core radius of $r_{\text{core}} = 1 \times 10^{-3} \text{ pc}$. The dotted line corresponds to the Schwarzschild radius of a $10^{12} M_{\odot}$ SMBH, and the dashed line corresponds to *HST* FWHM of typical filter from measurements made by the CANDELS collaboration https://irsa.ipac.caltech.edu/data/COSMOS/images/candels/hlsp_candels_hst_cos-tot_readme_v1.0.pdf. Bottom: The deflection angle α in function of radius for a point mass and our dPIE formalism. We can see a complete overlap after 1 arcsec lens a profile.

arcsec at $z = 0.2$, which adequately captures the gravitational potential of an SMBH. The bottom panel shows the deflection angle computed for our profile and a point mass, we can see that after 0.01 pc ($\sim 1 \text{ arcsec}$ at $z = 0.2$) the deflection angle is identical to a point mass.

We compute the shear and convergence profile from this compact dPIE to demonstrate that it is an appropriate representation of the point mass. We find that the kappa profile, following the density profile presented in Fig. 1, reaches ~ 0.1 after 0.02 arcsec – extremely similar to the lensing behaviour produced by the analytical point mass profile used by Karamazov et al. (2021) and Karamazov & Heyrovsky (2022). We remind the reader that the convergence for a point mass is zero everywhere except at its location. The shear profile for a point mass and our dPIE are nearly identical to < 1 per cent after 20 pc (or 0.001 arcsec for a lens at $z = 0.2$). Therefore, we argue that our choice of dPIE profile offers a reasonable and robust representation to model both a central and a wandering SMBH with an associated residual stellar component resulting from the tidal stripping/merging of an infalling galaxy into the cluster environment.

Within this setting, the mass of the dPIE profile is set entirely by the velocity dispersion, σ . Following the formula derived from Elíasdóttir et al. (2007) equations (A11) and (A25), we have:

$$\sigma_{\text{dPIE}}^{\text{SMBH}} = \sqrt{M_{\text{bh}} * \frac{4G}{6\pi} * \frac{r_{\text{cut}}}{(r_{\text{cut}}^2 - r_{\text{core}}^2)}} \approx \sqrt{\frac{M_{\text{bh}}}{r_{\text{cut}}} * \frac{4G}{6\pi}}. \quad (9)$$

3 LENSING BY THE CENTRAL BCG SMBH

We first examine the lensing effects produced by the massive SMBH hosted at the centre of the cluster BCG. As noted by Karamazov & Heyrovsky (2022), the inclusion of a point-like mass at the centre of the cluster BCG potential can strongly affect the resulting lensing configurations. Karamazov et al. (2021) distinguish two regimes where formally the ratio of the convergence produced by the BCG to that of the SMBH exceeds 10^{-4} , when a single NFW profile is used to model the BCG and a point-like source the SMBH.

Our empirical, observationally based approach does not make such distinctions of regimes based on the convergence, and instead we focus on the ratio of measured quantities – the mass ratio between different contributors to the overall mass budget. Highlighted in Fig. 2, we show how significantly a point-like mass can affect the lensing configuration that is produced. For a host galaxy with a total total mass of $10^{12} M_{\odot}$ (as computed following Elíasdóttir et al. 2007) with an increasing value of central black hole mass, we show the effect in the left column, for the case of an isolated galaxy (not embedded in the cluster environment); in the middle panel for a galaxy in a smoothed dPIE potential mimicking a central SMBH in a cluster BCG with a total mass of $5 \times 10^{14} M_{\odot}$ ($\sigma_{\text{dPIE}} = 552 \text{ km s}^{-1}$, $r_{\text{core}} = 30 \text{ kpc}$, $r_{\text{cut}} = 1500 \text{ kpc}$) and in the rightmost panel, the same galaxy now embedded instead in an NFW halo with a total mass of about $3.8 \times 10^{14} M_{\odot}$. Increasing the mass of the central SMBH in the galaxy produces the remarkable effect of boosting the radial caustic curve (blue diamond) outside the tangential caustic curve in the case of a dPIE profile (two left columns). In the case of the SMBH at the centre of a cluster scale potential (middle column), the area occupied by the radial caustic goes from 0.4 arcsec^2 for an SMBH mass of $10^9 M_{\odot}$ to 5 arcsec^2 for an ultramassive $10^{10} M_{\odot}$ SMBH. The outer critical curve is only slightly boosted. A similar boosting effect is not observed for the case of the NFW profile cluster halo (right column). In this case, the most noticeable effect that appears is the splitting of the radial critical curves for a massive enough cluster. For the case shown in Fig. 2 such rare and exotic catastrophic configurations appear only when the SMBH mass is tuned up to reach $M_{\text{SMBH}} = 3.50 \times 10^{10} M_{\odot}$ (see Schneider, Ehlers & Falco 1992; Orban de Xivry & Marshall 2009 for more details on rare lensing geometries). The ellipticity of the cluster scale halo can influence the mass of when the splitting of the radial critical curve occurs, as higher elliptical profile increase the density in one direction, we documented two cases for which we vary the ellipticity in Appendix A, Fig. A1.

4 LENSING SIGNALS OF CENTRAL SMBHS IN CLUSTER GALAXIES

In this section, we study the lensing effect of an SMBH hosted at the centre of a cluster member galaxy. Due to the lensing boost from the underlying larger scale cluster components, stronger effects can be produced as explained below. For exploring these effects, we start with modelling the underlying environment with a mock cluster. We add a single cluster scale halo and sub-halos to mimic the contribution of cluster member galaxies. Due to the sensitivity

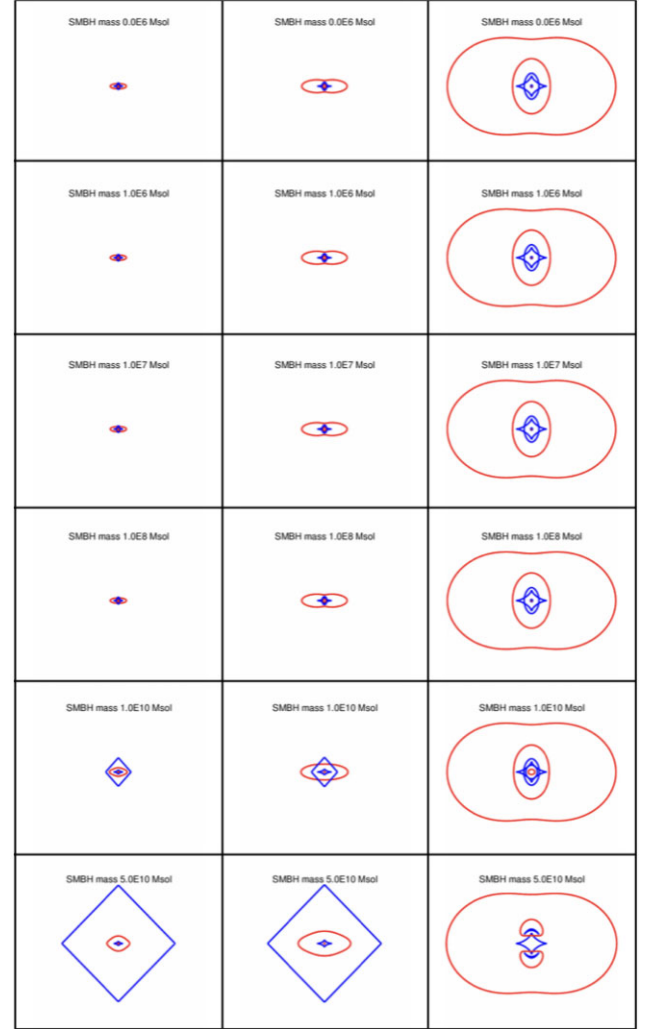


Figure 2. Lensing configurations for a galaxy with a total mass of $10^{12} M_{\odot}$ ($r_{\text{core}} = 0.1 \text{ kpc}$, $r_{\text{cut}} = 50 \text{ kpc}$, $\sigma_{\text{dPIE}} = 135 \text{ km s}^{-1}$, and ellipticity = 0.8) hosting a central SMBH with varying mass (mass increasing from top to bottom) in different environments. *Left:* isolated field galaxy – *middle:* dPIE in a cluster environment with the larger scale component characterized by ellipticity = 0.1, $r_{\text{core}} = 30 \text{ kpc}$, $r_{\text{cut}} = 1500 \text{ kpc}$, and $\sigma_{\text{dPIE}} = 552 \text{ km s}^{-1}$ yielding a total mass $M_{\text{tot}} = 5 \times 10^{14} M_{\odot}$ – *right:* SMBH embedded in a larger scale cluster modelled with an NFW profile characterized by the following parameters: $c = 7$, $r_s = 200 \text{ kpc}$, ellipticity = 0.1, and a total mass of $M_{200} = 3.8 \times 10^{14} M_{\odot}$. It is seen that at specific mass, the SMBH embedded in an NFW profile splits the internal critical curve (two lowest panels of the right column). This transition occurs in this configuration for a mass of $M_{\text{SMBH}} = 3.50 \times 10^{10} M_{\odot}$. Each box has a length of 20 arcsec aside, corresponding to 66 kpc at $z = 0.2$. Further explorations of the lensing configurations produced by a range of SMBH masses are available at: <https://sites.google.com/view/guillaume-mahler-astrophysicist/per-animation/paper-animation-central-smbh>.

of the lensing signal to the parameters of the mass models, we used a realistic lens model of an observed cluster lens and rearrange the cluster member locations keeping their radial distances unchanged in multiple realizations. The main dark matter central velocity dispersion and cut radius have been slightly reduced to match a total mass of $5 \times 10^{14} M_{\odot}$. The final model used here is

available online.¹ We now include an SMBH with mass as expected from the empirical scaling relations at the centre of cluster member galaxies.

4.1 Effects of central SMBHs on the lensing configurations

The combined lensing power of the cluster, the host galaxy and its central SMBH are now studied in detail. We identify two main cases and the resulting lensed image geometries. The first case is when the host galaxy lies outside the main cluster critical curve, as illustrated in Fig. 3. In this scenario, the cluster member galaxy produces its own critical curve. The principal effect for such a configuration appears to be the disappearance of the radial critical curve of the galaxy, similar to the effect studied in the case of isolated individual galaxy lenses (e.g. Mao et al. 2001). However, due to the lensing boost from the cluster, even less massive galaxies can produce large enough critical curves to potentially produce detectable image configurations. Secondly, a more spectacular effect appears when the host galaxy is situated inside the main cluster critical curve. In this case, the cluster member galaxy’s critical curve serves in practice as the radial critical curve for the overall cluster. Increasing the mass of the SMBH for such configurations, we find, first creates a cassinoid shape (peanut-like) before splitting the curve into two separate rounded critical curves as seen in the left column of Fig. 3. This unique configuration would offer a compelling case to look for a central SMBH in a cluster member galaxy in the inner core region of a cluster-lens. However, upon varying the SMBH mass, we note that the mass needed for such an event to occur is high and in the case displayed Fig. 3 this appears for an SMBH at about $10^9 M_{\odot}$. Such a high mass corresponds to the existence of an overmassive SMBH in a $10^{12} M_{\odot}$ host galaxy (an outlier away from the typical relation (Gültekin et al. 2009), however, such cases have been reported (van den Bosch et al. 2012).

4.2 Statistical effects of central SMBHs on the shear profile of sub-haloes

Masses of sub-haloes in clusters have been detected from statistically combining detected strong and weak lensing signals (Pastor Mira et al. 2011; Natarajan et al. 2017; Niemiec et al. 2018; Sifón et al. 2018). Future surveys from the LSST Vera Rubin observatory, or the *Nancy Grace Roman Telescope* are expected to overcome statistical limitations by detecting a large population of hitherto undetected massive cluster lenses. We investigate the potential statistical signature of the central SMBHs in stacked shear profiles of cluster member galaxies. We use our mock cluster presented in Section 4 associating every cluster member galaxy with a central SMBH following equation (8). We produce a shear profile at the location of every cluster member and stack the signal for bright galaxies, corresponding to the luminosity range $M^* - 1 < m_{\text{gal}} < M^* + 1$. We then compare the profiles for the same selected galaxies for the realization without a central SMBH. In addition, we compare the stacks with the signal derived for the known degenerate case altering the internal structure for the cluster galaxies with a modified core radius, from $r_{\text{core}}^* = 0.15$ kpc with the signal using a smaller core $r_{\text{core}}^* = 0.05$ kpc and a larger core with $r_{\text{core}}^* = 0.5$ kpc. In our simulation, we use the same scaling relations with luminosity for the core radius $r_{\text{core}} = r_{\text{core}}^* (L/L^*)^{1/2}$, as adopted in several previous works by Jullo et al. (2007), Richard et al. (2010), and Mahler et al.

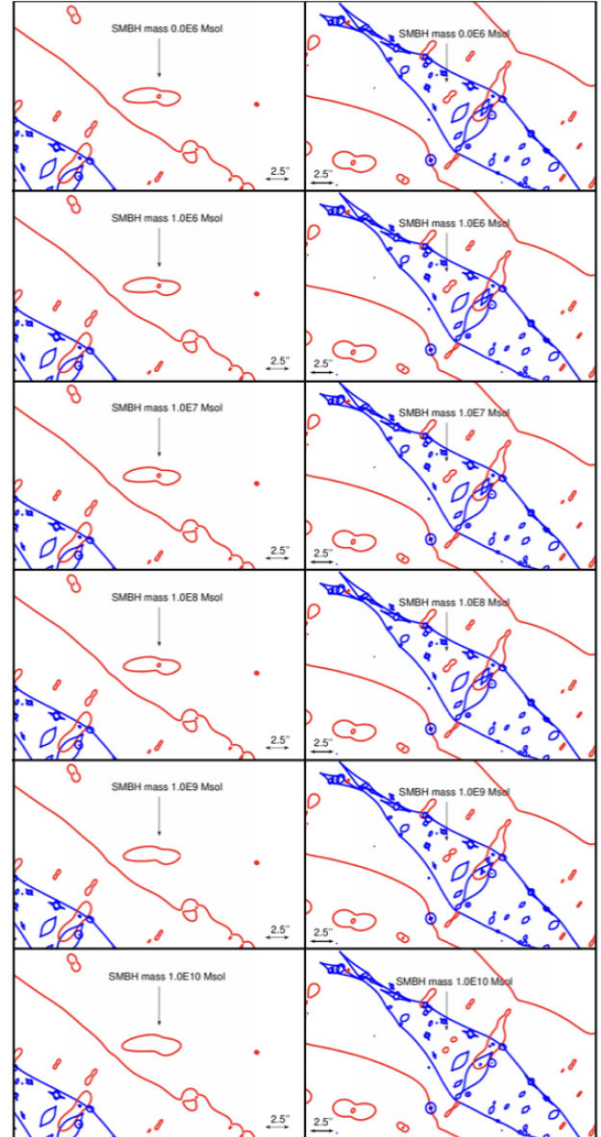


Figure 3. Lensing configurations produced by galaxies with increasing mass of the central SMBH from top to bottom: 0, 10^6 , 10^7 , 10^8 , 10^9 , $10^{10} M_{\odot}$. The SMBH is located at the centre of each frame, at centre of the galaxy pointed by the arrow *Left*: $10^{12} M_{\odot}$ galaxy with central SMBH placed outside the cluster’s main critical line. The main effect of a massive SMBH is to remove the central critical curve of the galaxy. *Right*: $10^{12} M_{\odot}$ galaxy placed inside the main critical line of the large-scale cluster. In this case, the effect of increasing the mass of the SMBH leads to the shrinking of the central part of the galaxy’s critical line leading to eventually causing it to split into two. Each box shown is 20 arcsec on a side. Further explorations of the lensing configurations as a function of SMBH masses are available at: <https://sites.google.com/view/guillaume-mahler-astronomer/paper-animation/paper-animation-centralsmbhcluster>.

(2018, 2019). Fig. 4 shows the stacked shear profiles, where it is clearly seen that the effect on the shear profile arising from changing the core radius of the galaxy far exceeds the effect of adding in an SMBH. Therefore, we conclude that the statistical lensing signature of a central SMBH in the shear profile is degenerate with that of the properties of the stellar component in the inner regions of cluster member galaxies and hence not discernible.

¹<https://sites.google.com/view/guillaume-mahler-astronomer/lens-model>

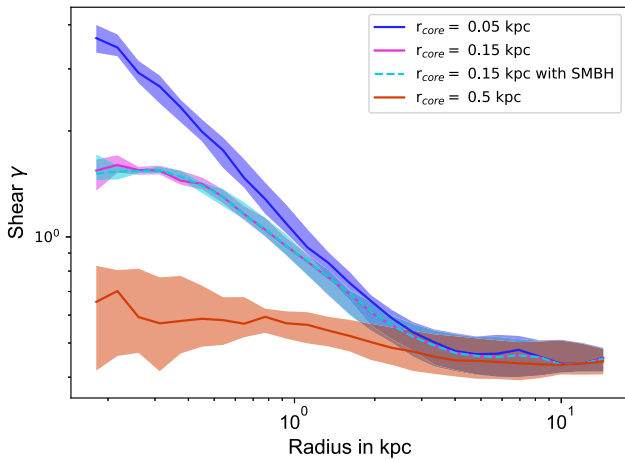


Figure 4. The stacked shear profile of the bright cluster member galaxies: bright cluster members galaxies are defined as those with a magnitude m , in the range $M^* - 1 < m < M^* + 1$. The solid lines represent galaxies without an SMBH, but with varying core radius. From top to bottom the core radii are 0.05, 0.15, and 0.5 kpc. The dotted line corresponds to the shear profile with a central SMBH hosted by cluster member galaxies. The shaded region represents the 1σ asymmetric distribution of shear strength for bright galaxies, with and without a central SMBH.

5 LENSING SIGNALS OF WANDERING SMBHS

In addition to the wandering population of SMBHs detected in the high-resolution simulated cluster Romulus-C that includes the dark matter and the baryon component (Tremmel et al. 2019), dark matter only simulations also reveal the existence of massive structures within the cluster-scale haloes, that could also be interpreted as free-floating black holes Banik et al. (2019). Two mechanisms could originate the wandering SMBH population. First, infalling galaxy is the main mechanism of clusters growth and only a fraction of the galaxy survive. While being completely stripped out of their stars in their infall from tidal friction (Wu et al. 2013; Hagggar et al. 2022), the remaining central black hole can survive and stay within the haloes without enough stars around it to be directly detected. A second mechanism is the ejection of an SMBH due to recoil as described in Paynter & Thrane (2022). To implement our solution we radially distribute wanderers following a lognormal distribution as a function of projected clustercentric radius as reported in Ricarte et al. (2021a) (see Fig. 6 in their analysis) with a mean at $0.1 R_{200}$ (radius at 200 times the critical density of the Universe) of the host haloes. In this work, we use a cluster host halo of $5.10^{14} M_{\odot}$ and a $R_{200} = 1.5$ Mpc. In the high-resolution simulated cluster Romulus-C studied by Ricarte et al. (2021a), they report finding over 1600 wanderers distributed within the virial radius. In accordance with this demographic, we randomly draw 1000 locations for our wanderers.

We repeat this mock cluster simulation a 1000 times following the mass and positions described above. To mimic realistic scenarios, we choose to limit ourselves to a mass range of 10^6 – $10^{10} M_{\odot}$ for the SMBH masses. Following these constraints, we numerically computed the probability for the presence of massive SMBH. There is 3.7 per cent probability that at least one SMBH wanderer with a mass above $10^8 M_{\odot}$ acts as a lens and this probability drops to 0.07 per cent to have at least two SMBHs above $10^8 M_{\odot}$. The probability for at least 1 SMBH to be more massive than $10^9 M_{\odot}$ is about 0.02 per cent (or 1 per 5000 clusters).

6 SMBH LENSING SIGNATURES IN SPECIFIC MULTIPLE IMAGE CONFIGURATIONS

Observationally detectable lensing signatures of a SMBH or for a compact dark matter halo without a sufficiently luminous counterpart exhibit a large variety of image configurations. The most obvious cases emerge when a SMBH is near a critical curve or when its impact is boosted by significant amplification from the larger-scale cluster host halo. In the following section we summarise the five distinct categories of potential observational signatures of lensing by a SMBH:

- (i) Image splitting due to alignment of the SMBH inside the cluster critical curve.
- (ii) Change in the observed flux of one of the lensed images.
- (iii) Apparent skewing in the light profile (or velocity field) and an apparent break in symmetry.
- (iv) Apparent increase in the size of a single lensed image
- (v) Apparent disappearance of an internal image

We detail each of these categories further in the following subsections.

6.1 Image splitting due to alignment of the SMBH inside the cluster critical curve.

The presence of an SMBH introduces a perturbation in the lensing configurations as noted. If the image of the lensed source is exactly aligned with the SMBH the resulting image is split. The perfect alignment represents the maximum splitting that SMBH can generate, that we refer to that later as the splitting power. Fig. 5 illustrates the splitting power of SMBHs as a function of their mass. This splitting power is mainly driven by the actual mass of the SMBH, other contributing factors are redshift, a smaller variation appears with increasing redshift of the source (up to 25 per cent for redshift 10); the underlying magnification (up to 10 per cent for an order of magnitude change in magnification) and the cluster induced shear (up to 25 per cent). From Fig. 5, we clearly see that an SMBH of more than $10^8 M_{\odot}$ has a large enough splitting power to be detected by *HST*. However, we note here that the size of the caustic curve in the source plane is small. For example, at $z = 2$, a source in alignment with a $10^8 M_{\odot}$ SMBH, needs to have distinct feature emitting light smaller than ~ 100 pc. If the light source is homogeneous and covers a larger area, an observer cannot identify the two separate components. This would result in observations similar to the one detailed in Section 6.4.

6.2 Change in the observed flux of one of the lensed images

In the case of perfect alignment between the SMBH and the lensed sources, the produced image can be split. Using the same mock simulation, we measure the flux within a 1.0 arcsecond radius aperture around the image of the source. We find that the apparent change in flux depends greatly on the mass of the SMBH and the underlying magnification of the host cluster. We attempt to quantify the de-magnifying effect and derive the decrements in the flux ratio. Fig. 6 shows the de-magnification as a function of magnification boost from the cluster ranging from 1.7 to 30, when the SMBH and image remains well within the cluster’s internal critical curve.

We note that the underlying magnification is more important for a massive SMBH for low magnifications. We interpret this as a consequence of the regime where the underlying properties of the SMBH dominates. For underlying magnifications $\gtrsim 9$ the detected

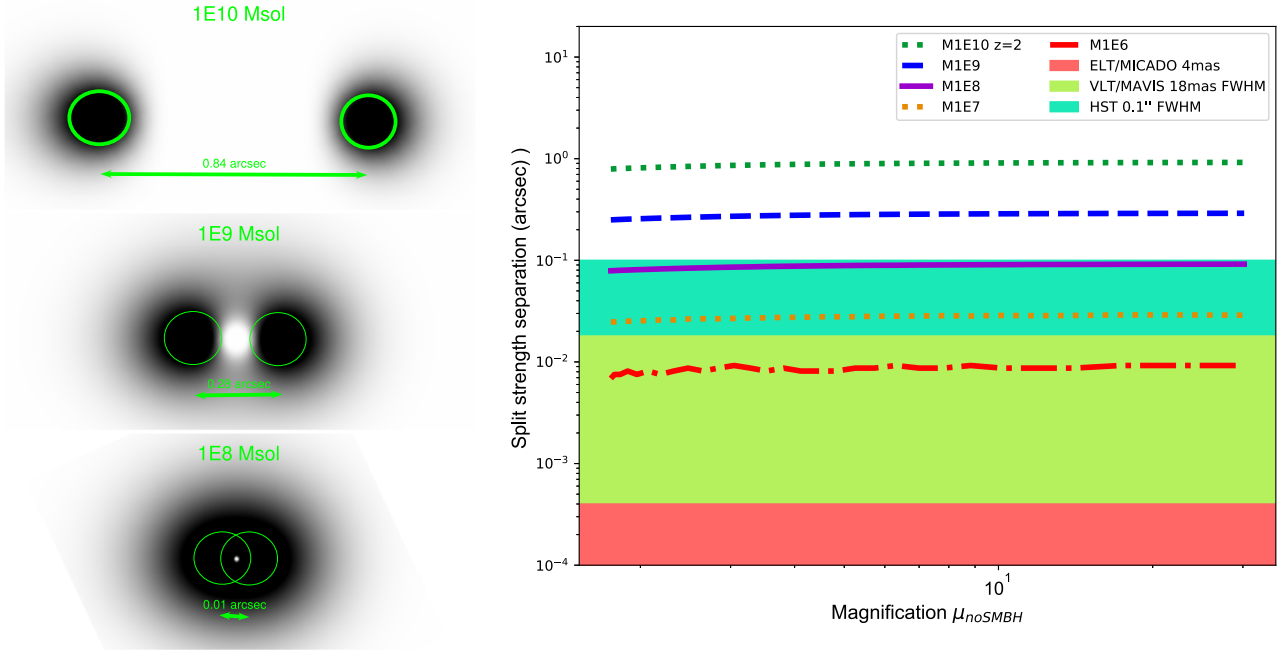


Figure 5. This figure shows the splitting power of an SMBH. *Left:* Illustration of the splitting of the image by an SMBH in a $z = 0.2$ cluster of a $\sigma_G = 0.1$ arcsec Gaussian source at $z = 2$ (corresponding to 0.85 kpc), from top to bottom the mass of the SMBH is varied ranging from $10^{10} M_\odot$, to $10^9 M_\odot$, to $10^8 M_\odot$. *Right:* separation of the image split plotted as a function of the underlying cluster magnification for different masses of the SMBH. We see that while a massive SMBH can be detected easily with *HST* resolution data, even the effect of an SMBH that is a few times $10^7 M_\odot$ is potentially detectable providing there is perfect alignment. We also highlight here that the future VLT/MAVIS instrument will reach 18-mas resolution and the promised sampling of ELT/MICADO can reach 4 mas, bringing the resolution down to levels that might permit capabilities to detect SMBH lensing in cluster environments.

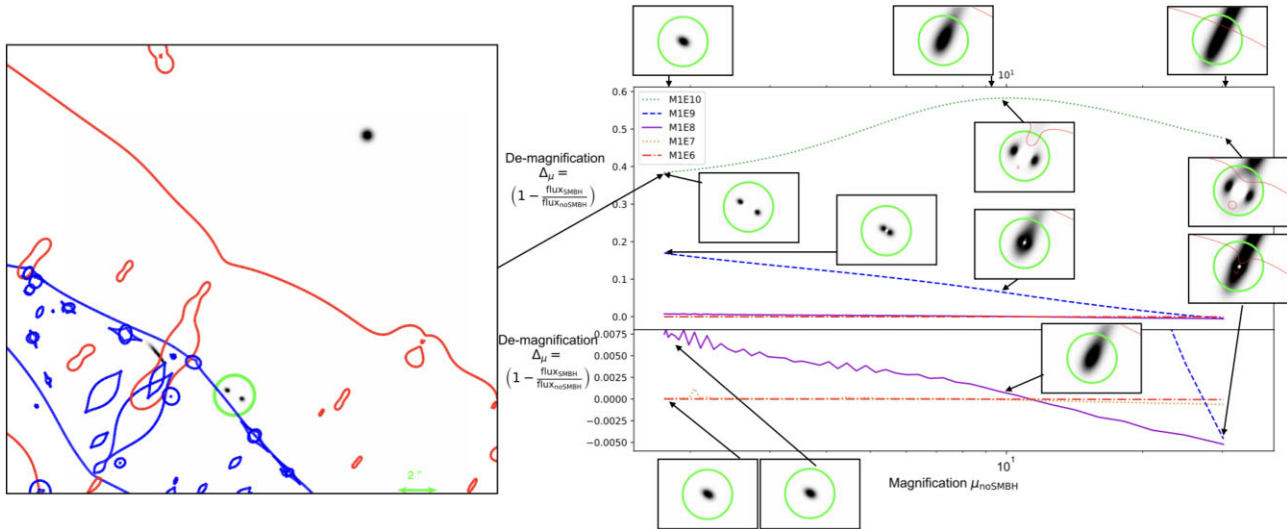


Figure 6. Simulation of a $z = 2.0$ $\sigma_G = 0.1$ arcsec Gaussian source at $z = 2$ (corresponding to 0.85 kpc) lensed by an SMBH in a $z = 0.2$ cluster. *Left:* Simulation of a source at $z = 2.0$ that appears to be de-magnified by a $10^{10} M_\odot$ SMBH, with its location marked as the green circle. The caustic and critical curves are shown in blue and red, respectively. The underlying magnification provided by the cluster is assumed to be a factor of 1.75. *Right:* The de-magnification induced by the presence of an SMBH within a circle of a 1 arcsec radius as a function of the underlying cluster-induced magnification. The de-magnification factor measures how much flux is lost compared to the case without the lensing effect of the SMBH. No instrumental effects have been added for these plots. Further explorations of the de-magnification as a function of the underlying cluster magnification are available at: <https://sites.google.com/view/guillaume-mahler-astronomer/paper-animation/paper-animation-demag>.

flux variation converges to only 1 per cent for all masses and magnifications. We note in our simulation that for masses below $10^8 M_\odot$, the effect on the flux is the nearly indistinguishable from the case with no SMBH. Only at much higher resolutions, in a

situation where the source is smaller than the caustic curve of the SMBH, does the effect of such a configuration become noticeable. We don't anticipate current and near future facilities to be able to have such resolving capabilities but the main challenge to measure

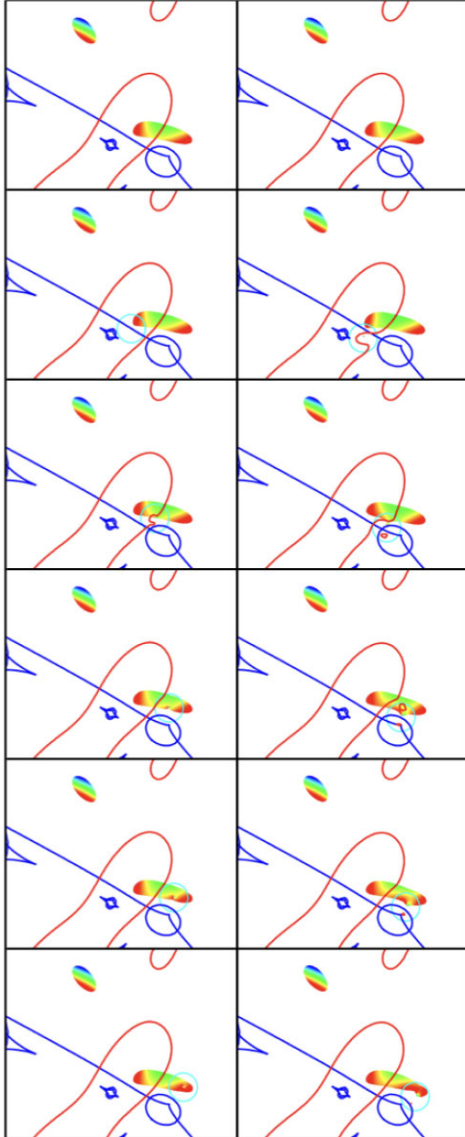


Figure 7. Light distribution distortion of a lensed sources modelled as a disc of 60 mas radius at $z = 2$ (corresponding to 0.5 kpc) as a function of the SMBH location and mass in a cluster at $z = 0.2$. The 0.3 arcsec radius (cyan circle) marks the location the SMBH. The blue and red curves mark the caustics and critical curves, respectively. The x -axis locations are the same for each panel and the y -axis locations for the left columns ($10^8 M_{\odot}$) are higher than for the right columns ($10^9 M_{\odot}$) for the effect of the SMBH to be seen. We notice how the presence of the SMBH distorts the image gradient. This would be visible either in the velocity field of the galaxy or potentially in looking at an unexpected symmetry between two images of the same sources, more easily identifiable in clumpy galaxies. Further exploration of the distortion as a function of SMBH location for a range of SMBH masses are available at <https://sites.google.com/view/guillaume-mahler-astronomer/paper-animation/paper-animation-warp>.

this effect might well be the accuracy of our mass modelling techniques.

6.3 Induced asymmetry with the skewing of the light profile and velocity field

The presence of SMBH wanderers aligned with sources will influence observed lensing configurations, detectable in the case of a

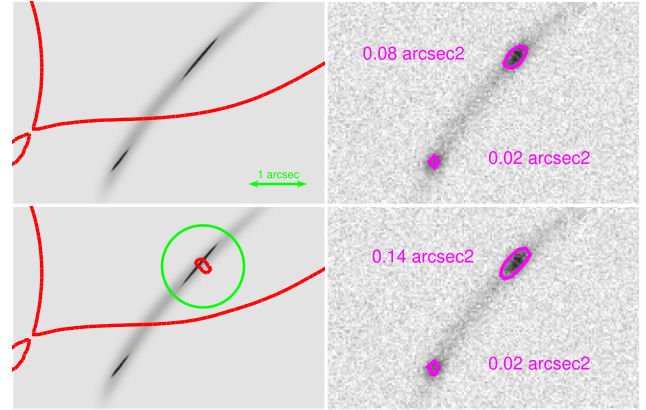


Figure 8. Simulation involving a two-component source: a compact ($\sigma_G = 1$ mas) and a larger ($\sigma_G = 7$ mas) Gaussian light distribution at $z = 2$ lensed by a cluster at $z = 0.2$. Top panels show the configuration without an SMBH and bottom panels with a $10^8 M_{\odot}$ SMBH at the location of the 1 arcsec radius (green circle). Left-hand panels show the simulation at infinite resolution and the right-hand panels show observations similar to what ACS/HST would observe (0.1 arcsec FWHM PSF, 30 mas pixel scale, with noise scaled as a 10 per cent of the maximum flux value). We see instrumental effects result in a larger area for the compact component, rendering it detectable.

source with enough resolution elements or a sharp gradient in colour, such as would be seen in a composite image of the velocity field. The presence and proximity of an SMBH can be detected by looking at the light distribution as shown in Fig. 7. Less massive SMBHs have a smaller area of influence and therefore need to be closer to the image to produce detectable effects. The detection of the presence of an SMBH is optimal for the configuration showed in Fig. 7 where the lensed image has a merging pair configuration and the SMBH is close to the critical curve. This warping of the image is also very similar to the effect induced by sub-haloes seen in galaxy–galaxy lensing events (e.g. Hezaveh et al. 2016). This effect might be the most common effect the SMBHs produce viz-a-viz lensing. At a constant underlying magnification, the strength of the warping is mainly affected by the distance between the lensed image and the SMBH. For instance, a $10^{10} M_{\odot}$ SMBH would have a significant effect up to ~ 0.5 arcsec away from the arc, a $10^9 M_{\odot}$ SMBH up to ~ 0.3 arcsec, and a $10^8 M_{\odot}$ SMBH up to ~ 0.1 arcsec.

6.4 Apparent increase in the size of one of the lensed images of a multiple

As discussed before, the more massive an SMBH the stronger impact it generates on the overall lensing configuration. In addition, for real observational facilities, taking into account additional effects such as the impact of the point-spread function, and pixel size or noise level also serve decrease our ability to precisely identify SMBH induced lensing configurations. However, even after instrumental effects are taken into account, the light distribution might reveal information to hint the presence of an SMBH. The primary effect would be to increase the apparent size of the image and this too preferentially in the lensing configuration where the SMBH influences an image outside the main cluster critical curve. Fig. 8 shows an example of the larger flux distribution induced by an SMBH ($M_{\text{SMBH}} = 10^8 M_{\odot}$). The source is modelled here as a double Gaussian to simulate the compact and broad emission components. The SMBH is placed outside the critical curve in this case. We note that in this example the area of the principal compact emission knot almost doubles. With a good prior

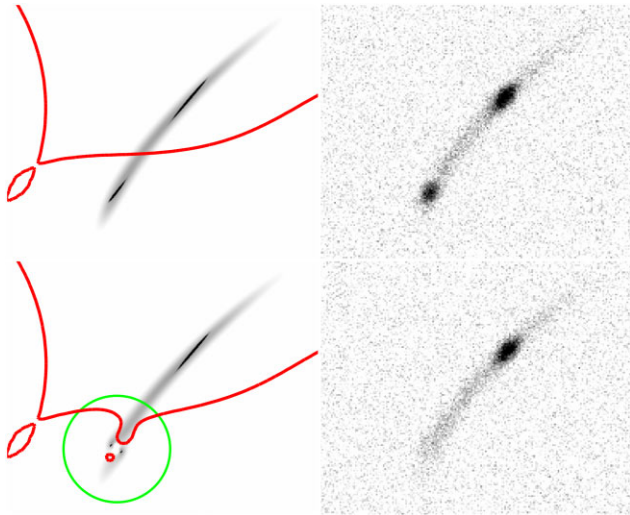


Figure 9. Simulation involving a two-component source: a compact ($\sigma_G = 1$ mas) and a larger ($\sigma_G = 7$ mas) Gaussian light distribution at $z = 2$ lensed by a cluster at $z = 0.2$. Top panels show the configuration without an SMBH in the cluster and bottom panels with a $10^9 M_\odot$ SMBH at the location of the 1 arcsec radius (green circle). Left-hand panels show the simulation at infinite resolution and the right-hand panels show the observation mimicking ACS *HST* observations (0.1 arcsec FWHM PSF, 30 mas pixel scale, with noise scaled as a 10 per cent of the maximum flux value). We see the instrumental effects result in the apparent disappearance of one of the images. The mass of the SMBH and the size of the source both contribute to this effect. We note that it prominently appear when the SMBH is near perfect alignment on of the image inside the cluster critical curve. Instrumental effects can more easily smooth the light distribution inside the cluster critical curve because the SMBH only split the image in two (instead of four outside).

understanding of the source light distribution such a measurement can lower the detectability threshold of SMBHs down to $M_{\text{SMBH}} = 10^8 M_\odot$ with *HST* specifications.

6.5 Apparent disappearance of the internal image

As discussed previously, the splitting power of an SMBH can separate images and therefore redistribute the light. When an SMBH is aligned almost exactly with the image of a lensed system inside the cluster critical curve the resulting effect is to separate the image into two (or into four if it happens to be outside the cluster critical curve). If the image is only split into two, instrumental and observational effects can affect their detectability resulting in the actual disappearance of one of the images. Fig. 9 highlights such situation. The PSF convolution and noise induced by the instruments, smooth the signal and make it harder to detect, giving an impression of the disappearance of the image and hence a break in the ‘typical’ image symmetry.

The apparent disappearance of the inner counter-images is the easiest case to detect in the upcoming large image survey data but this requires as noted a very tight alignment between the image and the SMBH and is therefore, expected to rare. In addition, it is degenerate with the large-scale cluster model and detailed source morphology.

7 OBSERVATIONAL TESTS

In this section, we explore for evidence of an SMBH in currently available lensing observations. While we did not find any clear-cut

evidence of SMBH lensing in our current fairly exhaustive search of peculiar lensing configurations, we found two cases where a wandering SMBH might provide a potentially plausible explanation to account for what is seen. As mentioned clearly at the start of our investigation, it is extremely challenging to pinpoint the role of an SMBH in any observed configuration as it is degenerate with the effect produced by a dark sub-halo. We want to stress here that tweaking other models not including SMBHs are also able to account for the observed data. However, the parameter space available to interpret the data is still open and it is in this context that we explore the possible role for SMBHs as lenses.

7.1 Asymmetrical lensing configuration in SGAS J003341.5+024217

The observational configuration of the arc shown in Fig. 10 is akin to the case referred in Section 6.4, though SMBH is required to be located on top of the critical curve. Fischer et al. (2019) report the asymmetrical lensing configuration for an arc at $z = 2.39$ merging on the critical curve. To model this case, here we include a wandering SMBH as a perturbation to account for the asymmetrical shape of this arc as shown in Fig. 10. The addition of the lensing perturbation from an SMBH allows us to reduce the rms positional error in the current best-fitting mass model of the system from 0.17 arcsec that does not include this additional degree of freedom of an SMBH, down to 0.01 arcsec including the SMBH. This improvement including this additional degree of freedom is real, as it is reflected in the value of the reduced χ^2 as well. Therefore, the inclusion of a wandering SMBH offers a plausible explanation for constructing a robust model for the observation.

7.2 Disappearance of lensing symmetry in RX J1347.5–1145

Richard et al. (2021) report a peculiar lensing configuration in a massive cluster observed with the combination of *HST* and MUSE. They identify unique compact continuum emission identified in *HST* and extended gas emission detected in MUSE that shows a large tail (see their fig. 12 or top panels of Fig. 11). With the lensing configuration from the authors’ published model, we would expect similar size for the extended tail on both sides of the critical curve. Here, we propose a different interpretation of the observations resembling the configuration studied in Section 6.5 where there is an apparent missing counter image. As reported earlier, a missing counter-image results when the source falls inside the cluster critical curve. Starting with the published models from Richard et al. 2021, we manually tweaked the main cluster model parameters to move the cluster critical curve to the middle of the lobe of the extended emission accomplished using an SMBH. We simulated the emission with two Gaussian distributions on top of each other, to represent the compact continuum emission with a circular Gaussian with $\sigma = 1$ mas and the Lyman α emission with an elliptical Gaussian with $\sigma_G = 18$ mas and $\sigma_g = 18$ mas for the semimajor and semiminor axis at a 90 deg angle from the horizontal direction. For a source at $z = 4.0840$ (Richard et al. 2021) this correspond to a 7 and 126 pc for the continuum and Lyman α emission, respectively, to mimic the Lyman α emission of the observed arc. The northern part of the extended emission is inside the cluster member critical curve and shows the compact continuum emission. We placed an SMBH on the southern part of the arc close enough such that cluster critical curves merge, effectively placing the SMBH inside the main cluster critical curve. This leads to the splitting of the compact emission component on the southern part of the arc. The inclusion of observational

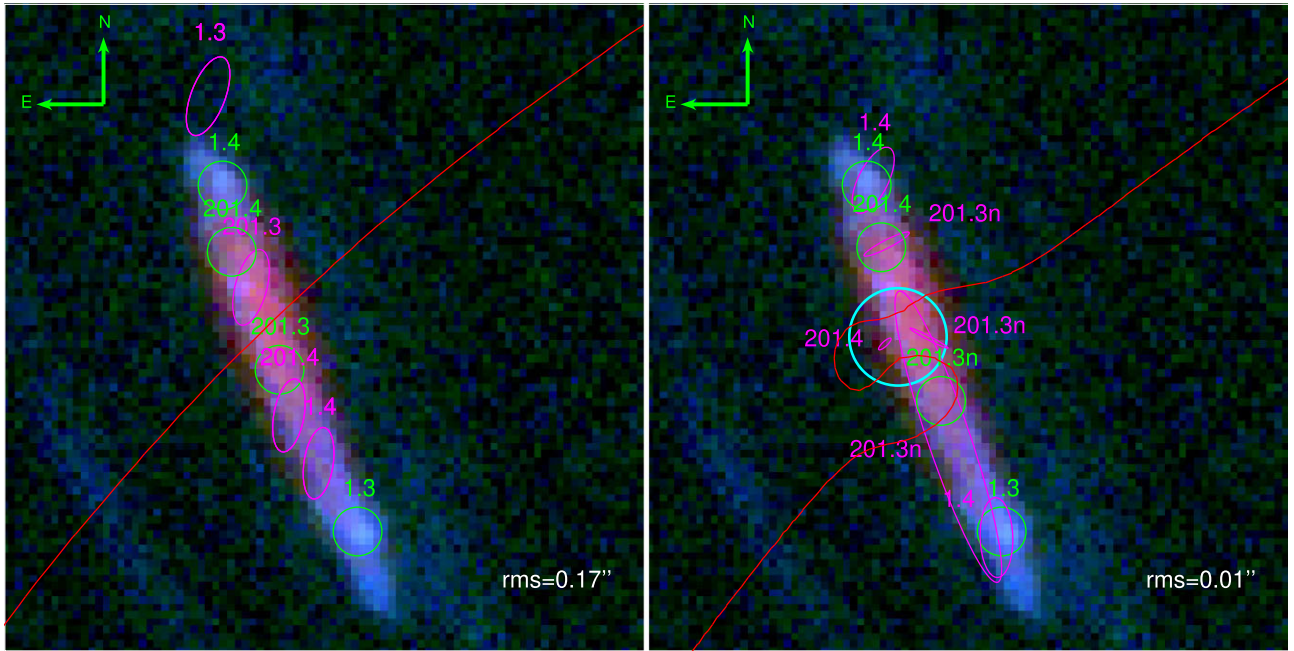


Figure 10. Previous analysis report that SGASJ003341.5+024217 show peculiar unexplained asymmetry (Fischer et al. 2019). *Left:* Original model; the lensing configuration is classically described as a merging pair, the critical curve (red curve) is passing through the centrally located red part of the system but the two extreme emission knots are not symmetrically located on each side of the critical curve as expected. *Left:* Alternative modelling including an SMBH at the location of the critical curve alleviate this tension. Our models that include a $4.7 \times 10^8 M_{\odot}$ SMBH at the location of the cyan circle (0.2 arcsec radius) perturbed the lensing critical curve to reestablish symmetry on both side of the curvy line. The green circle represents the emission knot on the image and the magenta circle are the corresponding predictions from the lens model.

effects causes the extended light emission to be smeared into a more elongated shape, reproducing the observation. We, therefore, conclude that with the addition of a $5 \times 10^8 M_{\odot}$ SMBH and a simple model for the source light distribution we can qualitatively reproduce the observations. The implication of lensing by an SMBH offers an alternative, viable interpretation. While this is by no means a claim for the detection of the lensing effect of an SMBH, it is simply a demonstration that inclusion of such a perturber offers a neat and natural explanation for the observed asymmetry seen in RXJ1347.5–1145.

8 CONCLUSIONS

Our analysis explores the observational lensing signatures of SMBHs in galaxy clusters. We model the mass of SMBHs as compact dPIE profiles and study their effect both as centrals hosted by cluster member galaxies as well as free-floating wanderers in the larger cluster environment. The presence of a population of wandering SMBHs in clusters has been recently claimed by Ricarte et al. (2021a) from the analysis of high-resolution cosmological simulations. Although the lensing effect of an SMBH is small, it imprints a discernible signature in unusual lensing image configurations, as summarized below:

(i) The presence of a central SMBH primarily affects the radial critical curve of its host, resulting either in its disappearance or by its splitting. Hint of a split critical curve would be a clear evidence for the presence of a central SMBH, but its detection remains challenging due to the overlap of the radial critical curve and the light of the lens itself. Large high-resolution radio surveys might be able to support a concerted search in the future due to the faintness of the emission from the lens at these wavelengths.

(ii) The shear induced by central SMBHs is statistically impossible to disentangle from the effect of a change in the density profile at the core of their host galaxies.

(iii) Wandering SMBHs can cause the disappearance of counter images. This effect would be the most obvious signature; however, it is also degenerate with the lensing properties of the larger scale cluster mass model as well as complexities in the intrinsic morphology of background sources.

(iv) Outside the cluster critical curve, the typical effect of a wandering compact SMBH would result in the asymmetric elongation of one of the images. This might be much a more common occurrence but to conclusively confirm the presence of the SMBH, a detailed lens model and careful source reconstruction is required to show this anomaly in the reconstructed image.

(v) The changes induced by wandering SMBHs in the light distribution of lensed sources can be tracked in the case of a obvious change in the symmetry of the field, ideally traced where clear gradients exist, such as in the velocity field of a lensed galaxy. Observing this feature requires robust mapping of the true velocity field of the source.

We attempt in this analysis to reconcile previously reported peculiar lensing configurations in SGASJ003341.5+024217 and RXJ1347.5–1145 by including perturbations induced by an SMBH into the mass models. With these new composite mass models, we do not claim detection or discovery of the presence of an SMBH, but rather demonstrate that a class of models with SMBHs ($M_{\text{SMBH}} = 4.7 \times 10^8 M_{\odot}$) might be able to alleviate some of the previously noted tensions in modelling these unusual lensing configurations.

We report that the ideal configurations that would reveal the presence of an SMBH without doubt would be the appearance of

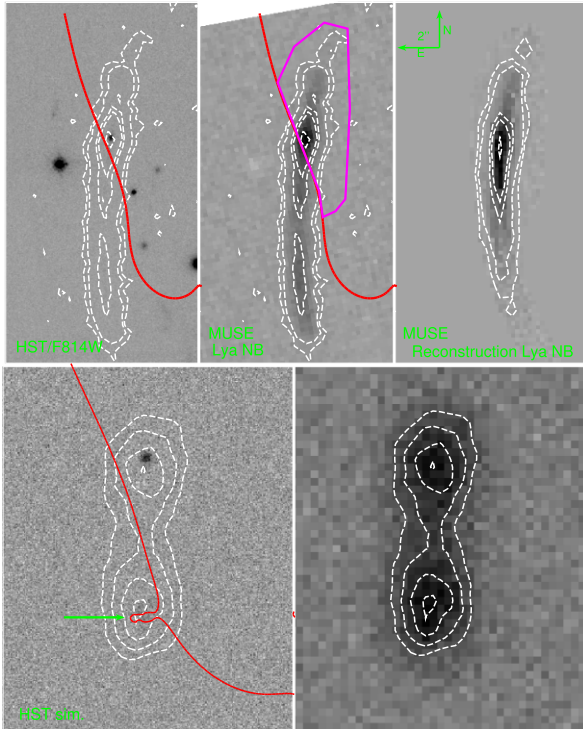


Figure 11. Alternative explanation for the peculiar lensing configuration in the multiply imaged system in RX J1347.5–1145. *Top:* The panels show system 25 (as reported in Richard et al. 2021) in the *HST*/F814W band (left), MUSE narrow band images centered on the Lyman α sources (middle) and a lens re-projection of the top part of the MUSE NB image Lyman α emission. This re-projection consist of selecting the pixels in the magenta polygon on the top left panel, sending them to the source plan and projecting them back to the image plan, showing the flux distribution assume with this lens model. The bottom part of the system does not match the expected lensing symmetry highlighted by the critical curve at the redshift of the images shown in red. *Bottom:* Our model offer alternative explanation of the lensing configuration: we slight modify the large-scale mass component to shift the critical curve to lie in between the two Lyman α peak. In addition, we include a $5 \times 10^8 M_{\odot}$ SMBH at the location of the green arrow showing as a ‘kink’ in the critical curve. We model the continuum emission from *HST* with a simple Gaussian with $\sigma_G = 1$ mas and the Lyman α emission with a elliptical Gaussian with $\sigma_G = 18$ and $\sigma_G = 18$ mas for the semimajor and semiminor axis at a 90 deg angle from the horizontal direction. This peculiar configuration accounts for the disappearance of the continuum peaky emission due to the ‘splitting’ of the image as noted in Section 6. The diffuse emission, because of the combined effect of it’s larger size and larger seeing mocked here with an FWHM = 0.5 arcsec), appear slightly more elongated on the lower portion of the diffuse emission, as in the observation.

a two-image split inside the cluster critical curves. We have not been able so far to identify such a split in observational data currently in hand. In the future, two complementary strategies can be pursued to discover wandering SMBHs. Future large surveys by the Rubin LSST Observatory, *Euclid*, or the *Nancy Grace Roman Telescope* will offer orders of magnitude more targets and will likely therefore uncover rare events of massive SMBH alignment. The second strategy would be to point extremely high resolution cameras on giant arcs and/or multiply imaged systems of clumpy galaxies to push down on the granularity of the mass distributions and hence the mass threshold of detectable SMBHs.

ACKNOWLEDGEMENTS

GM acknowledges funding from the European Union’s Horizon 2020 research and innovation programme under the Marie Skłodowska-Curie grant agreement No MARACHAS - DLV-896778. PN acknowledges the Black Hole Initiative (BHI) at Harvard University, which is supported by grants from the Gordon and Betty Moore Foundation and the John Templeton Foundation. PN acknowledges useful conversations with Angelo Ricarte and Michael Tremmel. MJ is supported by the United Kingdom Research and Innovation (UKRI) Future Leaders Fellowship ‘Using Cosmic Beasts to uncover the Nature of Dark Matter’ (grant number MR/S017216/1).

DATA AVAILABILITY

The data underlying this article are available in the article and in its online supplementary material. <https://sites.google.com/view/guillame-mahler-astronomer/paper-animation>

REFERENCES

- Banik U., van den Bosch F. C., Tremmel M., More A., Despali G., More S., Vegetti S., McKean J. P., 2019, *MNRAS*, 483, 1558
- Chen M. C., Broadhurst T., Lim J., Diego J. M., Ohya Y., Ford H., Benítez N., 2018, *ApJ*, 863, 135
- Collett T. E., Smith R. J., 2020, *MNRAS*, 497, 1654
- Dahle H. et al., 2013, *ApJ*, 773, 146
- Dai L., Miralda-Escudé J., 2020, *AJ*, 159, 49
- Diego J. M. et al., 2018, *ApJ*, 857, 25
- Elíasdóttir Á. et al., 2007, preprint ([arXiv:0710.5636](https://arxiv.org/abs/0710.5636))
- Event Horizon Telescope Collaboration, 2019, *ApJ*, 875, L1
- Ferrarese L., Merritt D., 2000, *ApJ*, 539, L9
- Fischer T. C. et al., 2019, *ApJ*, 875, 102
- Gebhardt K. et al., 2000, *ApJ*, 539, L13
- Gültekin K. et al., 2009, *ApJ*, 698, 198
- Haggar R., Kuchner U., Gray M. E., Pearce F. R., Knebe A., Yepes G., Cui W., 2022, *MNRAS*, in press
- Hezaveh Y. D. et al., 2016, *ApJ*, 823, 37
- Inada N., Oguri M., Falco E. E., Broadhurst T. J., Ofek E. O., Kochanek C. S., Sharon K., Smith G. P., 2008, *PASJ*, 60, 27
- Jullo E., Kneib J. P., Limousin M., Elíasdóttir Á., Marshall P. J., Verdugo T., 2007, *New J. Phys.*, 9, 447
- Karamazov M., Heyrovsky D., 2022, *ApJ*, 927, 101
- Karamazov M., Timko L., Heyrovsky D., 2021, *ApJ*, 922, 72
- Kassiola A., Kovner I., 1993, *ApJ*, 417, 450
- Keeton C. R., 2003, *ApJ*, 582, 17
- Kelly P. L. et al., 2018, *Nat. Astron.*, 2, 334
- Kneib J.-P., Natarajan P., 2011, *A&AR*, 19, 47
- Magorrian J. et al., 1998, *AJ*, 115, 2285
- Mahler G. et al., 2018, *MNRAS*, 473, 663
- Mahler G. et al., 2019, *ApJ*, 873, 96
- Mao S., Witt H. J., Koopmans L. V. E., 2001, *MNRAS*, 323, 301
- Martinez M. N. et al., 2022, preprint ([arXiv:2209.03972](https://arxiv.org/abs/2209.03972))
- Minor Q., Kaplinghat M., Chan T. H., Simon E., 2021a, *MNRAS*, 507, 1202
- Minor Q., Gad-Nasr S., Kaplinghat M., Vegetti S., 2021b, *MNRAS*, 507, 1662
- Muller S., Jaswanth S., Horellou C., Martí-Vidal I., 2020, *A&A*, 641, L2
- Natarajan P., Kneib J.-P., 1997, *MNRAS*, 287, 833
- Natarajan P. et al., 2017, *MNRAS*, 468, 1962
- Niemiec A. et al., 2018, *MNRAS*, 477, L1
- Orban de Xivry G., Marshall P., 2009, *MNRAS*, 399, 2
- Ostrovski F. et al., 2018, *MNRAS*, 473, L116
- Pastor Mira E., Hilbert S., Hartlap J., Schneider P., 2011, *A&A*, 531, A169
- Paynter J., Thrane E., 2022, preprint ([arXiv:2210.03267](https://arxiv.org/abs/2210.03267))

- Quinn J. et al., 2016, *MNRAS*, 459, 2394
 Ricarte A., Tremmel M., Natarajan P., Zimmer C., Quinn T., 2021a, *MNRAS*, 503, 6098
 Ricarte A., Tremmel M., Natarajan P., Quinn T., 2021b, *ApJ*, 916, L18
 Richard J. et al., 2010, *MNRAS*, 404, 325
 Richard J. et al., 2021, *A&A*, 646, A83
 Rusin D., Keeton C. R., Winn J. N., 2005, *ApJ*, 627, L93
 Schneider P., Ehlers J., Falco E. E., 1992, *Gravitational Lenses*, XIV. Springer-Verlag, Berlin, Heidelberg, New York
 Sharon K. et al., 2017, *ApJ*, 835, 5
 Sifón C., Herbonnet R., Hoekstra H., van der Burg R. F. J., Viola M., 2018, *MNRAS*, 478, 1244
 Smith R. J., Collett T. E., 2021, *MNRAS*, 505, 2136
 Smith R. J., Lucey J. R., Edge A. C., 2017, *MNRAS*, 467, 836
 Tamura Y., Oguri M., Iono D., Hatsukade B., Matsuda Y., Hayashi M., 2015, *PASJ*, 67, 72
 Tremaine S. et al., 2002, *ApJ*, 574, 740
 Tremmel M. et al., 2019, *MNRAS*, 483, 3336
 Werner M. C., Evans N. W., 2006, *MNRAS*, 368, 1362
 Winn J. N., Rusin D., Kochanek C. S., 2004, *Nature*, 427, 613
 Wong K. C., Suyu S. H., Matsushita S., 2015, *ApJ*, 811, 115
 Wong K. C., Ishida T., Tamura Y., Suyu S. H., Oguri M., Matsushita S., 2017, *ApJ*, 843, L35
 Wu H.-Y., Hahn O., Wechsler R. H., Behroozi P. S., Mao Y.-Y., 2013, *ApJ*, 767, 23
 van den Bosch R. C. E., Gebhardt K., Gültekin K., van de Ven G., van der Wel A., Walsh J. L., 2012, *Nature*, 491, 729

APPENDIX A: ELLIPTICITY OF THE CLUSTER HALO

Following our analysis on lensing configurations for different profile and masses of SMBH as described in Fig. 3. We quickly document here two cases of the influence of the cluster scale halo ellipticity on the lensing configurations for a combinations of three mass. A cluster halo simulated as an NFW, parametrized as $c = 7$, $r_s = 200$ kpc giving a total mass of $M_{200} = 3.8 \times 10^{14} M_\odot$, a host galaxy parametrized with a dPIE ($r_{\text{core}} = 0.1$ kpc, $r_{\text{cut}} = 50$ kpc, and SMBH with two masses $M_{\text{SMBH}} = 1 \times 10^8 M_\odot$ and $M_{\text{SMBH}} = 1 \times 10^{10} M_\odot$. We can notice that the critical at the centre is able to split at an earlier mass than the cases report in Fig. 2, if the cluster scale halo show a high enough ellipticity.

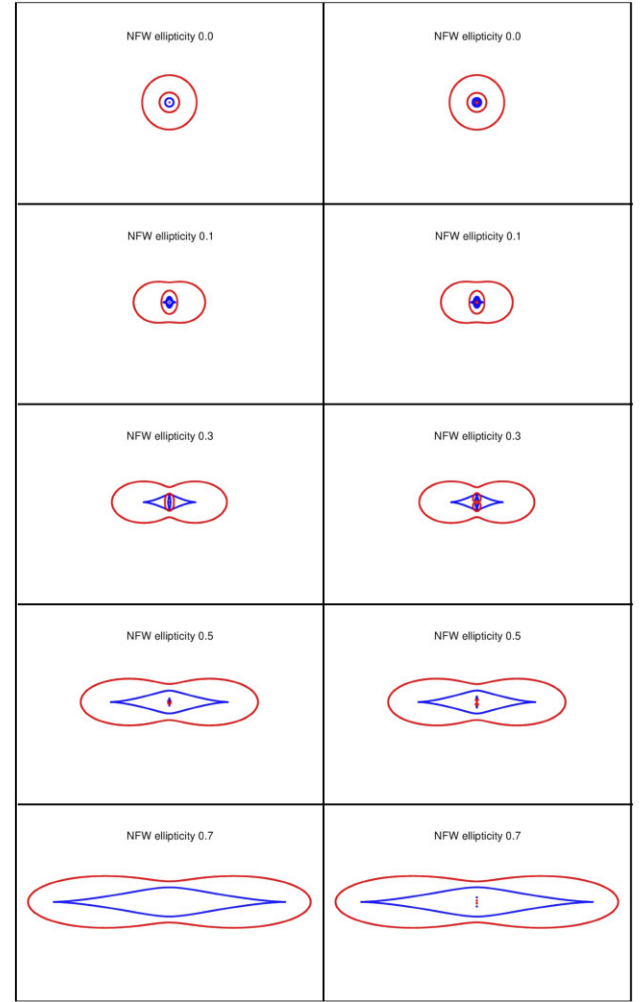


Figure A1. Lensing configurations for a $10^{12} M_\odot$ galaxy at the centre of an NFW profile with varying ellipticity for two different mass of central SMBH. An SMBH mass of $M_{\text{SMBH}} = 1 \times 10^8 M_\odot$ for the left column and $M_{\text{SMBH}} = 1 \times 10^{10} M_\odot$ on the right column. The NFW profile characterized by the following parameters: $c = 7$, $r_s = 200$ kpc and a total mass of $M_{200} = 3.8 \times 10^{14} M_\odot$. The host galaxy is parametrized with a dPIE ($r_{\text{core}} = 0.1$ kpc, $r_{\text{cut}} = 50$ kpc, $\sigma_{\text{dPIE}} = 135 \text{ km s}^{-1}$) and has a total mass $10^{12} M_\odot$. We can see that the ellipticity plays a role in the lensing configuration and can lower the mass when the internal critical curve split into two part as detailed in Fig. 3. Each box has a length of 85 arcsec aside, corresponding to 280 kpc at $z = 0.2$.

This paper has been typeset from a $\text{\TeX}/\text{\LaTeX}$ file prepared by the author.